Two-Dimensional Phase Unwrapping Using a Block Least-Squares Method

Jarle Strand, Torfinn Taxt, *Member, IEEE,* and Anil K. Jain, *Fellow, IEEE*

***Abstract*—We present a block least-squares (BLS) method for two-dimensional (2-D) phase unwrapping. The method works by tessellating the input image into small square blocks with only one phase wrap. These blocks are unwrapped using a simple procedure, and the unwrapped blocks are merged together using one of two proposed block merging algorithms. By specifying a suitable mask, the method can easily handle objects of any shape. This approach is compared with the Ghiglia–Romero method and the Marroquin–Rivera method. On synthetic images with different noise levels, the BLS method is shown to be superior, both with respect to the resulting gray values in the unwrapped image as well as visual inspection. The method is also shown to successfully unwrap synthetic and real images with shears, fiber-optic interferometry images, and medical magnetic resonance images. We believe the new method has the potential to improve the present quality of phase unwrapped images of several different image modalities.**

***Index Terms*—Interferometric images, magnetic resonance images, phase unwrapping.**

I. Introduction

PHASE unwrapping is the task of finding the true phase values, given the wrapped phase values in an image. The origin of the task is due to the fact that in a number of imaging applications only the wrapped, or principal, phase values can be measured or directly computed. The principal phase values are restricted to the interval $(-\pi, \pi]$. For example, in complex valued images, only the principal phase values can be computed from the real and imaginary parts using the arctangent function. Formally, if a true phase value is denoted as ϕ, then the measured or computed value is $\Psi = W(\phi)$. The wrap function W is defined as $W(\phi) = \phi + 2\pi r$, where r is an integer such that $-\pi < W(\phi) \leq \pi$. Fig. 1(a) shows a synthetic phase image where the pixel values are defined by a parabolic function, and Fig. 1(b) is the corresponding wrapped image obtained by using the wrap function on each pixel in the original image. In practice, it is the wrapped image that is observed, and the problem is to reconstruct the unwrapped image. This is usually a difficult inverse problem because of the noise that invariably degrades all real data, and of undersampling of the data in areas where the true phase values changes rapidly (e.g., lay-overs in SAR interferometry).

There are many important imaging applications requiring two-dimensional (2-D) phase unwrapping. In synthetic aperture radar (SAR) interferometric imaging, the phase values correspond to the terrain elevation height [1]–[4]. A similar application is fiber-optic interferometry, where the phase values represent the depths of the imaged object at the sample points [5]. Magnetic resonance (MR) images can be created with pulse sequences so that the phase values contain information about flow or inhomogeneities in the main magnetic field [6]–[8]. The important complex cepstrum transform requires phase unwrapping as one of the processing steps [9]. Other applications are compensated imaging [10] and speckle imaging [11].

The above applications have stimulated the development of several phase-unwrapping methods. There are four major categories of methods: integration-based [3], [6], [12]–[14], least-squares based [2], [15]–[21], model-based [22], [23], and Bayesian-based [1], [24]. Common to most of the methods is the estimation of the local derivatives in the images. If the true phase differences between adjacent samples in an image are less than π, then the derivatives are correctly estimated by using discrete differentiation and the wrap function [25]. Given the derivatives in the horizontal and vertical directions, the unwrapped image may be found by a discrete integration. This is the basis for the integration methods [12]. Because of noise and discontinuities in the images, the requirements for the estimation of the derivatives are often not met. Direct integration approaches will, therefore, fail in many real-world applications. There are numerous methods that try to detect the areas where the derivatives can not be estimated, and then avoid using these areas in the integration process [3], [6], [13], [14]. The least-squares methods minimize the squared error between the observed and the estimated image. The origin of the least-squares methods is in the papers by Fried [16] and Hudgin [17]. For these methods, a solution can be found directly by using Fourier series methods [17]. Hunt describes the least-squares approach in the framework of linear algebra, and it is seen that the problem is equivalent to solving the discrete version of the Poisson partial differential equation [18]. This makes it possible to solve the unwrapping problem using the ensemble of methods available for solving the Poisson equation [26], [27]. Ghiglia and Romero use the discrete cosine transform (DCT) and the conjugate gradient (CG) methods [19]. The fast Fourier transform (FFT) is used by Pritt and Shipman [20]. A least-squares method with

Manuscript received June 11, 1997; revised January 29, 1998. This work was supported by the Research Council of Norway. The associate editor coordinating the review of this manuscript and approving it for publication was Dr. Ping Wah Wong.

J. Strand and T. Taxt are with the Department of Physiology, Section for Medical Image Analysis and Pattern Recognition, University of Bergen, 5009 Bergen, Norway (e-mail: j.strand@interpro.no; torfinn.taxt@pki.uib.no).

A. K. Jain is with the Pattern Recognition and Image Processing Laboratory, Department of Computer Science, Michigan State University, East Lansing, MI 48824 USA (e-mail: jain@cps.msu.edu).

Publisher Item Identifier S 1057-7149(99)01556-0.

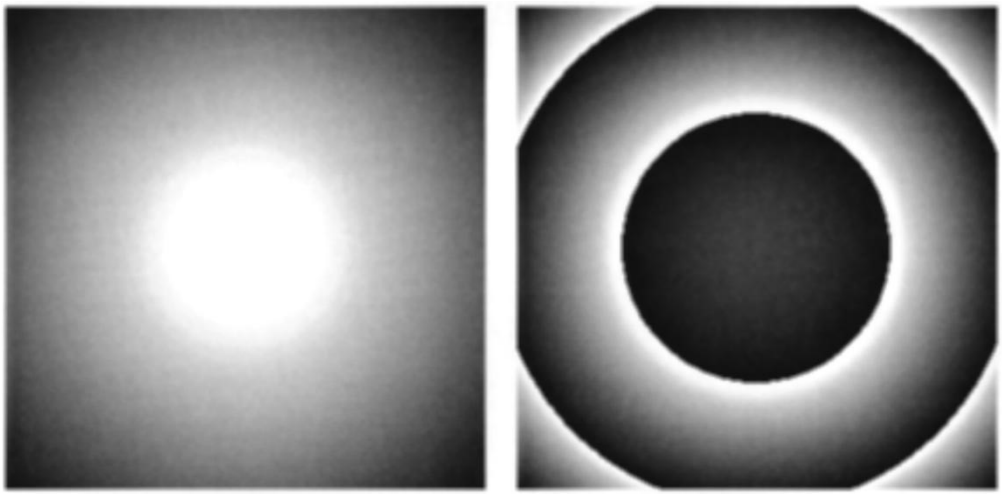

(a) (b)

Fig. 1. Example of phase wrapping. (a) True phase image and (b) observed wrapped image.

regularization is proposed by Marroquin and Rivera [21]. Fornaro *et al.* [2] presents a method based on Green's first identity. This method is theoretically equivalent to the least-squares-based methods [15]. Model-based methods assume that the image to be unwrapped can be described by some model, usually a polynomial surface [22], [23]. The Bayesian methods put the problem in the context of Bayesian restoration, and the knowledge about the surface to be unwrapped is then given by a prior distribution [1], [24].

In this paper, a new method for phase unwrapping of 2-D images is presented and evaluated. By tessellating the input image into small squares that only contain one phase wrap, it is possible to directly unwrap each block by a simple operation. The blocks are then merged together using a least-squares error approach between the blocks. Only multiples of 2π are added or subtracted to the wrapped input image. Thus, the method maintains the integrity (congruence modulo 2π) of the input data. The method is very fast, and robust to noise since the unwrapping is performed on all the pixels in the blocks simultaneously.

The paper is organized as follows. The new phase unwrapping method is described in the next section. Then, the least-squares methods of Ghiglia and Romero (GR method) [19], and of Marroquin and Rivera (MRM method) [21] are presented. These two methods are used in the evaluation of the new method, and were chosen because they are relatively stable to noise. The experimental design is given thereafter, followed by evaluation results. Finally, in the discussion, the noise sensitivity of the BLS method is discussed and the evaluation results are analyzed.

II. The Block Least-Squares Method

In real-world images, there is always stochastic noise that prevents accurate estimation of the derivatives for all the pixels in the images. The noise is a problem for all phase unwrapping methods. For example, for the least-squares methods, the consequence of the noise is that the pixel values are not added or subtracted an integer multiple of 2π, but instead adjusted with a fractional value to minimize the least squares sum. The integrity of the input phase values are thus corrupted. We have developed a noise robust method that maintains the integrity of the input data by exploiting the properties of the Riemann surface for the complex logarithmic function.

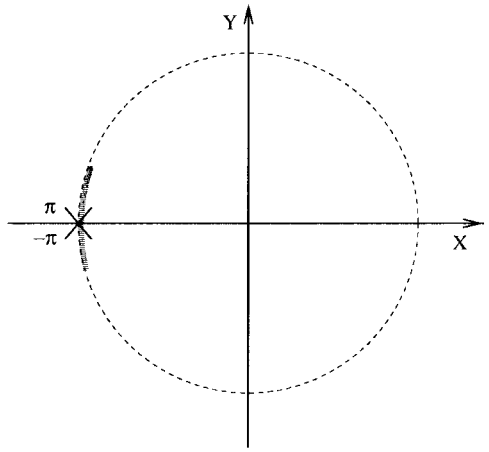

Fig. 2. Phase values on the complex plane.

A. Definitions and Initialization

The input image Ψ contains the wrapped phase values and is defined on the $M \times N$ lattice

$$Z = \{\mathbf{s} = (x, y): 0 \leq x < M, 0 \leq y < N\}. \quad (1)$$

In order to process objects of any shape, a mask $\Lambda \subset Z$ must be specified. The elements in Λ are the pixels of the input image that contain data corresponding to the object of interest. Such masks can be found by thresholding extracted quality maps [28]. Alternatively, for complex valued images, a simple thresholding of the corresponding amplitude images often produces good masks. In specific applications, different methods for producing masks should be considered to find the best possible masks.

The first step of the method is to tessellate the input image into small square blocks of size $m \times n$. For simplicity, we assume that m is a divisor of M, and that n is a divisor of N. Each block is a subset of Z which we denote as

$$B_{k,l} = \{(x, y) \in Z: \\ km \le x < (k+1)m, \ln \le y < (l+1)n\} \quad (2)$$

where

$$0 \le k < K, \qquad K = M/m, \\ 0 \le l < L, \qquad L = N/n. \quad (3)$$

The blocks are divided into four categories; *full, empty, partial,* and *split*. A block $B_{k,l}$ is full if $B_{k,l} \cap \Lambda = B_{k,l}$, and empty if $B_{k,l} \cap \Lambda = \emptyset$. Connected component analysis [29] with the first-order neighborhood system is performed on all the other (nonfull and nonempty) blocks. Blocks with more than one connected component are split blocks; the others are partial blocks. The different block types are processed in different ways in each step of the algorithm.

B. Block Unwrapping

The input image must be sampled dense enough so that each block $B_{k,l}$ contains a maximum of one phase wrap, i.e., the true phase values for each block must be in an interval $[a, b)$ such that $|b - a| < 2\pi$. This assumption makes it possible to unwrap each block directly by using the following operator on every pixel (x, y) in the block

$$\hat{\Psi}_{x,y} = W[\Psi_{x,y} + \rho] - \rho \quad (4)$$

where $\Psi_{x,y}$ is the observed wrapped phase value at point (x, y), W is the wrap function defined in the introduction, and ρ is a constant specific for each block. ρ must be in the interval $[0, 2\pi)$. Clearly, (4) subtracts exactly 2π or does not change the input value. The purpose of the ρ inside the wrap function W is to shift the wrap position, and thus rotate possible phase wraps out of the blocks. The ρ outside the wrap function makes sure that we only change the input data by integer multiples of 2π.

It is essential to understand (4) in order to understand the whole method. We will therefore explain this equation in some detail. If we, for demonstration purposes, assign to each wrapped phase value $\Psi_{x,y}$ the complex number $e^{i\Psi_{x,y}}$ (which is equal to setting the amplitude to one), it becomes possible to plot the phase values on the unit circle in the complex plane. Fig. 2 shows the complex plane, where the shaded area indicates the plot interval for the phase values of a given block. The wrap position is along the negative part of the x-axis. Obviously, the plotted block contains a phase wrap, since the shaded interval is located on both sides of the wrap position. When we unwrap phase images, we assume that the values are not restricted to the complex plane. The unwrapped phase values cannot, therefore, be plotted on the complex plane. Instead, the phase values are points on the complex Riemann surface for the complex logarithmic function [30]. The observed wrapped phase image is then the projection of the image from the complex Riemann surface for the complex logarithmic function, onto the complex plane. Again, for simplicity, we set the amplitude of the complex numbers to one. The phase values are now points on the spiral depicted in Fig. 3(a). The phase wrap of the example block plotted in Fig. 2 is now clearly visible, since the shaded interval has been split into two pieces. The ρ inside the wrap function in (4) rotate the values on the spiral. Fig. 3(b) shows the result after a small positive ρ has been added to all the phase values in the block. Notice that the uppermost of the two shaded areas is now outside the principal interval. When the wrap function is applied, the result is one continuous interval [Fig. 3(c)]. By finally performing a reverse rotation, i.e., to subtract ρ from the phase values, the values are rotated back so that the projection onto the complex plane is the same as for the original phase values [Fig. 3(d)]. This shows how (4) can be used to unwrap the blocks of the image.

To unwrap a block $B_{k,l}$ is now equivalent to finding a suitable value for ρ. The method uses the ρ that minimizes the penalty function $t_{k,l}$, given by

$$t_{k,l} = \frac{1}{\#S^x_{k,l}} \sum_{S^x_{k,l}} \left| \hat{\Psi}_{x,y} - \hat{\Psi}_{x-1,y} \right| \\ + \frac{1}{\#S^y_{k,l}} \sum_{S^y_{k,l}} \left| \hat{\Psi}_{x,y} - \hat{\Psi}_{x,y-1} \right| \quad (5)$$

where

$$S^x_{k,l} = \{(x, y): \{(x, y), (x-1, y)\} \subset \Lambda \cap B_{k,l}\}, \\ S^y_{k,l} = \{(x, y): \{(x, y), (x, y-1)\} \subset \Lambda \cap B_{k,l}\} \quad (6)$$

and $\#(\cdot)$ is the unary function giving the number of members in a set. The idea here is to minimize the sum of the absolute values of the first order differences in the blocks. Since the phase wraps give high first-order differences, a low value of $t_{k,l}$ is likely to represent a block without phase wraps.

The full and partial blocks can be directly unwrapped. For split blocks, the minimization has to be done on each connected component in the blocks separately. The empty blocks need of course no processing.

Fig. 4(a) shows a noisy wrapped image. The temporary result after each block is unwrapped is shown in Fig. 4(b).

C. Block Merging

After each block is successfully unwrapped, the blocks must be merged together to form the unwrapped image. For each block, the merging consists of adding an integer multiple r of 2π to each pixel in the block, so that the blocks fit together. We propose two merging methods. The first is a direct method which can be used for images with valid data in all the pixels, i.e., $\Lambda = Z$. The other method is for unwrapping objects of arbitrary shape, and is based on heuristics.

1) Direct Merging: For the direct merging we order the blocks by setting $B_i = B_{k,l}$, where $i = kL + l$. At first, none of the blocks have assigned fixed values. The values in the first block B_0 are kept as they are, and we define the set of blocks with assigned fixed values to be $U = B_0$. The rest of

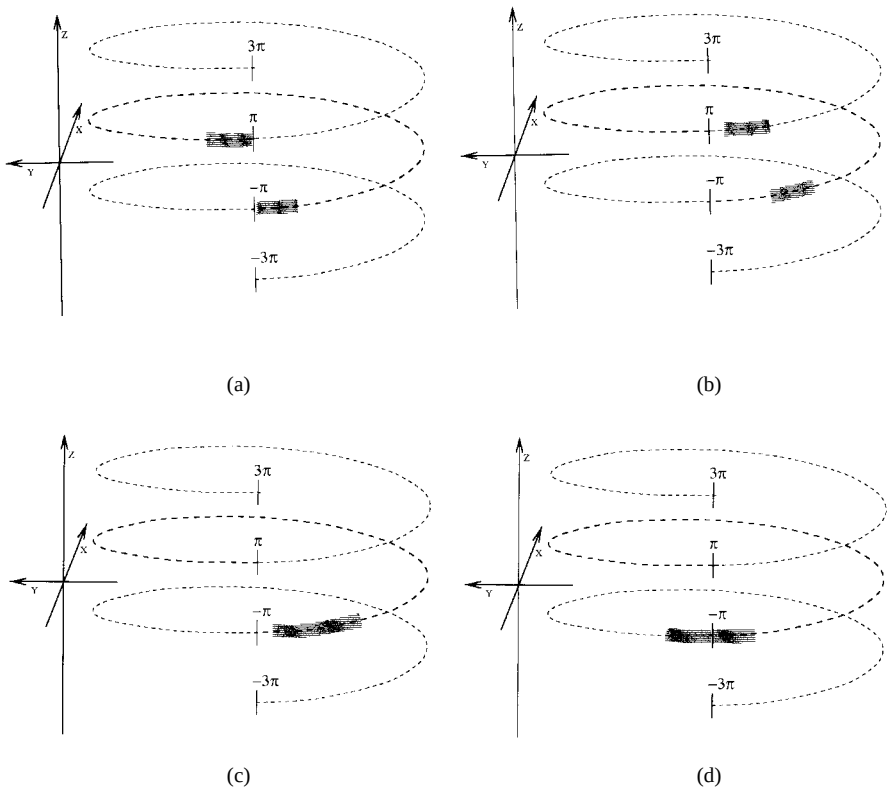

(a) (b)

(c) (d)

Fig. 3. Block unwrapping. (a) Phase values on the complex Riemann surface for the complex log function. (b) Rotated phase values (by a small ρ value). (c) Rotated and wrapped phase value. (d) Rotated, wrapped, and inverse rotated phase values.

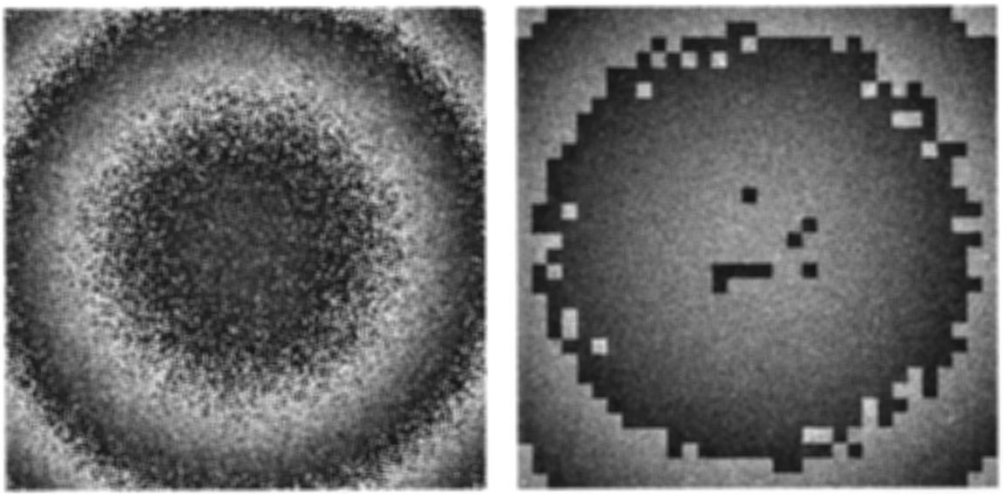

(a) (b)

Fig. 4. Block unwrapping. (a) Noisy wrapped image. (b) Temporary result with blocks unwrapped.

the blocks are processed in consecutive order. For each block B_i, we define

$$A_i = \{(c_i, d_i) \in Z^2 \colon c_i \in U,\, d_i \in B_i,\, c_i \sim d_i\} \tag{7}$$

where $c_i \sim d_i$ denotes that the pixels c_i and d_i are first-order neighbors. The pixel values in the block must be adjusted so that the block fits with the blocks in U. This is done by adding an integer number r of 2π to every pixel in B_i. We use a least-squares fit, and find r by minimizing

$$Q = \sum_{A} \left(\hat{\Psi}_{c_i} - \hat{\Psi}_{d_i} + 2\pi r\right)^2 \tag{8}$$

which is equivalent to

$$r = \text{Round}\left(\frac{\sum_{A}\left(\hat{\Psi}_{c_i} - \hat{\Psi}_{d_i}\right)}{2\pi \# A}\right) \tag{9}$$

where Round$(\cdot)$ is the function that returns the closest integer to the argument. We set $U = U \cup B_i$, and continue with the block B_{i+1} until all the blocks have been processed.

2) Merging Heuristics: The following heuristics are used. For each connected component in the mask, choose a full block as the starting point. If there are no full blocks, choose a partial block. Split blocks are handled separately in the end. The phase values in the starting block are kept as they are, and the block is marked as assigned a value. An iterative procedure is used to *grow* the area of assigned blocks. Let U denote the set of blocks with assigned values, and N_U be the set of full or partial blocks that are first-order neighbors to one or more blocks in U, and that are not members of U. For each iteration, a new block is added to U. The block to be added is the full block in N_U with the lowest $t_{k,l}$ value. If there are no full blocks in N_U, the partial block with the highest $\#(B_{k,l} \cap \Lambda)$ value is chosen. In cases where there are several blocks with the same highest $\#(B_{k,l} \cap \Lambda)$ value, the block with the lowest $t_{k,l}$ value is chosen among these. Let $B_{k,l}$ be the chosen block. Before $B_{k,l}$ can be added to U, a value $2\pi r$ must be added to all pixels in the block so that it fits with the blocks already in U. This is done with the same least-squares fit method as in the direct merging, but now the sets $A_{k,l}$ are defined as

$$A_{k,l} = \{(c_i, d_i) \in Z^2 \colon c_i \in U, d_i \in B_{k,l} \cap \Lambda, c_i \sim d_i\}. \tag{10}$$

The pixel values in the block are updated by adding $2\pi r$, and we set $U = U \cup B_{k,l}$. When the iterations stop, the procedure is repeated for the other connected components in the mask. Finally, the split blocks are handled. A similar iterative approach is used. For each iteration, if a connected component with unassigned values has a corresponding nonempty set A, it is assigned a value using the above described least-squares fit method.

D. Implementation Details and Method Overview

The implementation is quite straightforward, except to find the optimal ρ values for (4). One simple method is to try a finite number of evenly spaced values in the interval $(0, 2\pi]$. We found that this method was sufficient for our images. It is also possible to use methods such as simulated annealing [31], or other methods designed to find global extrema of nonlinear functions.

The applied block sizes should be based on the image sampling density, the complexity of the imaged object, and the noise level. A large number of phase wraps compared to the sampling density requires a small block size. High noise levels should be compensated by a large block size. The computation requirements of the method increases with smaller block sizes. To find a suitable block size for a given image, we started with a large block size, and then gradually reduced the block size until the resulting image was successfully unwrapped. In general, it is hard to know when an image is correctly unwrapped. In practice, however, there often exist *a priori* knowledge about the imaged object. Based on this, a visual inspection is often sufficient to determine if the unwrapping is successful. When a block size was found for a given image, the same block size could be used on other images of the same modality, if they had a similar complexity.

The direct unwrapping method can be summarized as follows:

- Unwrap each block in the image using (4).
- Set $U = B_0$.
- FOR $i = 1$ to mn-1
  - — Find r for B_i using (9).
  - — Add $2\pi r$ to all pixels in B_i.
  - — Set $U := U \cup B_i$.
- END FOR

The heuristic unwrapping method can be summarized as follows:

- Divide the blocks into the four categories *full, partial, split,* and *empty*.
- Unwrap the nonempty blocks in the image using (4). For split blocks each connected component must be unwrapped separately. Empty blocks are kept unchanged.
- Set $U = \emptyset$
- WHILE there are full or partial blocks not in U
  - — Choose a full block that is not a member of U. If there are no full blocks, choose a partial block that is a not member of U. Let $B_{k,l}$ be the chosen block.
  - — Set $U := U \cup B_{k,l}$.
  - — WHILE N_U is not empty
    - ∗ Find the full block in N_U with the lowest $t_{k,l}$ value. If there are several blocks with the same lowest value, choose any one of them. If there are no full blocks in N_U, find the partial block with the highest $\#B_{k,l}$ value. If there are several partial blocks with the same highest $\#B_{k,l}$ value, choose the one with the lowest $t_{k,l}$ value among these. Let $B_{k,l}$ be the selected block.
    - ∗ Find r for $B_{k,l}$ using (9).
    - ∗ Add $2\pi r$ to all pixels in $B_{k,l}$.
    - ∗ Set $U := U \cup B_{k,l}$.
  - — END WHILE
- END WHILE
- Perform least-squares fit on each connected components in all split blocks. For each connected component, use (9) to find r, and then add $2\pi r$ to all pixels.

III. Global Least—Squares Methods

We give a short description of two phase unwrapping methods that will be used in the evaluation. The methods are least-squares-based and were proposed by Ghiglia and Romero [19] and by Marroquin and Rivera [21]. They were chosen for the evaluation because they are relatively stable to noise.

A. Ghiglia and Romero

This method assumes that the phase image is continuous, and that the sampling is dense enough so that the true phase values between two adjacent points do not differ by more than π.

The wrapped, principal, phase value is denoted Ψ, and ϕ is the true phase value. The phase differences in the horizontal and the vertical direction are estimated by

$$\begin{aligned}\Delta^x_{x,y} &= W(\Psi_{x+1,y} - \Psi_{x,y}),\\ \Delta^y_{x,y} &= W(\Psi_{x,y+1} - \Psi_{x,y})\end{aligned} \tag{11}$$

where W is the wrap function. The least-squares solution to the phase unwrapping problem is then the values $\phi_{x,y}$ that minimizes t.

$$\begin{aligned}t = &\sum_{x=0}^{M-2}\sum_{y=0}^{N-1}(\phi_{x+1,y} - \phi_{x,y} - \Delta^x_{x,y})^2\\ &+ \sum_{x=0}^{M-1}\sum_{y=0}^{N-2}(\phi_{x,y+1} - \phi_{x,y} - \Delta^y_{x,y})^2.\end{aligned} \tag{12}$$

This is equivalent to solving the following system of linear equations

$$\begin{aligned}&(\phi_{x+1,y} - 2\phi_{x,y} + \phi_{x-1,y}) + (\phi_{x,y+1} - 2\phi_{x,y} + \phi_{x,y-1})\\ &\quad = \rho_{x,y}\end{aligned} \tag{13}$$

where

$$\rho_{x,y} = (\Delta^x_{x,y} - \Delta^x_{x-1,y}) + (\Delta^y_{x,y} - \Delta^y_{x,y-1}) \tag{14}$$

which is a discretization of the Poisson partial differential equation [18].

The solution of (13) can be found for instance by using a particular 2-D DCT [32], or by using the 2-D discrete Fourier transform [20]. The solution in the DCT domain is given by

$$\hat{\phi}_{x,y} = \frac{\hat{\rho}_{x,y}}{2\left(\cos\dfrac{\pi x}{M} + \cos\dfrac{\pi y}{N} - 2\right)} \tag{15}$$

where $\hat{\rho}$ is the DCT domain representation of ρ. Estimates of the unwrapped phase values $\phi_{x,y}$ are found by taking the inverse DCT of $\hat{\phi}_{x,y}$. It should be noted that the DCT implies Neumann boundary conditions, i.e., the derivatives are assumed to be zero at the boundaries.

B. Marroquin and Rivera

Marroquin and Rivera extend the GR method by introducing regularization, thereby making the method more robust to noise. They define the subset $S \subset Z$ as the set where valid observations are available, and $D \subset Z$ as the set where the solution should be calculated.

The phase differences in the horizontal and vertical direction are given by

$$\begin{aligned}\delta^x_{x,y} &= W(\Psi_{x,y} - \Psi_{x-1,y}),\\ \delta^y_{x,y} &= W(\Psi_{x,y} - \Psi_{x,y-1}).\end{aligned} \tag{16}$$

This is similar to the differences in the GR method, except that backward differencing is used instead of forward differencing.

The operator $\mathcal{L}$ is taken to be a first-order difference, giving

$$\begin{aligned}||\mathcal{L}\phi - h||^2 = &\sum_{(x,y)\in S_x \cap D_x}[\phi_{x,y} - \phi_{x-1,y} - \delta^x_{x,y}]^2\\ &+ \sum_{(x,y)\in S_y \cap D_y}[\phi_{x,y} - \phi_{x,y-1} - \delta^y_{x,y}]^2\end{aligned} \tag{17}$$

where D_x, D_y, S_x, and S_y are sets that keep track of the boundary conditions.

The regularization operator P_2 is defined as a combination of second-order differences and given by

$$\begin{aligned}||P_2\phi||^2 = &a\sum_{(x,y)\in D_{xx}}[\phi_{x-1,y} - 2\phi_{x,y} + \phi_{x+1,y}]^2\\ &+ b\sum_{(x,y)\in D_{yy}}[\phi_{x,y-1} - 2\phi_{x,y} + \phi_{x,y+1}]^2\\ &+ c\sum_{(x,y)\in D_{xy}}[\phi_{x,y} - \phi_{x,y+1} - \phi_{x+1,y}\\ &\qquad + \phi_{x+1,y+1}]^2\end{aligned} \tag{18}$$

where D_{xx}, D_{yy}, and $D_{x,y}$ are sets that keep track of the boundary conditions. The parameter values are chosen to be $a = b = 1$, and $c = 2$. This corresponds to letting $||P_2\phi||^2$ represent a discrete approximation of the equilibrium potential energy of a thin plate. The cost function is now defined by

$$U(\phi) = ||\mathcal{L}\phi - h||^2 + \lambda||P_2\phi||^2. \tag{19}$$

The unwrapped phase solution is the set of phase values that minimizes the cost function. The solution is found by setting the derivative of U with respect to ϕ equal to zero, which leads to a discrete version of a fourth-order partial differential equation. Marroquin and Rivera show how this equation can be solved by using a particular DCT, and by the use of the conjugate gradient method [33]. When $\lambda = 0$, the method is the same as that of Ghiglia and Romero.

IV. Experimental Design and Evaluation Procedures

The BLS method was tested using three different experiments. The first experiment showed the robustness of the method using images of different linear phase gradients and noise levels. The next experiment was a numerical evaluation that compared the BLS method with the GR method [19] and the MRM method [21]. Finally, the versatility of the BLS method was demonstrated by unwrapping phase images of different image modalities.

TABLE I
BLS RESULTS (STANDARD DEVIATION) OF SLOPE TEST IMAGES, BLOCK SIZE 4

Slope	Noise standard deviation (σ)						
	0.00	0.25	0.50	0.75	1.00	1.25	1.50
	(0.00)	(0.25)	(0.50)	(0.75)	(1.00)	(1.22)	(1.42)
0.00	0.00	0.25	0.50	0.75	1.01	1.92	2.70
0.25	0.00	0.25	0.50	0.75	1.39	1.86	3.70
0.50	0.00	0.25	0.50	0.76	1.33	3.03	5.92
0.75	0.00	0.25	0.50	0.75	1.75	5.70	10.21
1.00	0.00	0.25	0.50	0.96	4.57	9.81	13.88

TABLE II
BLS RESULTS (STANDARD DEVIATION) OF SLOPE TEST IMAGES, BLOCK SIZE 8

Slope	Noise standard deviation (σ)						
	0.00	0.25	0.50	0.75	1.00	1.25	1.50
	(0.00)	(0.25)	(0.50)	(0.75)	(1.00)	(1.22)	(1.42)
0.00	0.00	0.25	0.50	0.75	1.00	1.25	1.46
0.25	0.00	0.25	0.50	0.75	1.01	1.26	2.07
0.50	0.00	0.25	0.50	0.83	1.64	2.77	6.40
0.75	0.00	0.51	5.72	9.91	11.19	13.30	13.32
1.00	14.96	14.79	14.94	15.27	15.69	16.29	17.80

A. Robustness

To get a good indication of the robustness of the BLS algorithm, we generated planar images (i.e., the intensities of the images were a simple linear function of the horizontal axis), and added different levels of Gaussian noise. (It can be argued that Gaussian noise is not the usual noise encountered in many phase images. For complex images, the phase is calculated from the real and imaginary parts, and is not Gaussian. However, if the amplitude of the complex images is large compared to the noise, and the noise in the real and imaginary channels are Gaussian, then the phase noise can be correctly approximated by a Gaussian distribution [34].) The images were of size 64 × 64 pixels. All combinations of slope values 0, 0.25, 0.50, 0.75, 1.0, and noise levels with standard deviations 0, 0.25, 0.50, 0.75, 1.0, 1.25, 1.5, were used. Since the noise was added to the unwrapped images, the effective standard deviations of the noise in the wrapped images were slightly smaller. In all tables the effective standard deviations are given in parenthesis. To evaluate the results, the standard deviations between the original noise free images, and the unwrapped result images, were calculated using this formula:

$$\sigma^2 = \frac{1}{MN} \sum_{x=0}^{M-1} \sum_{y=0}^{N-1} (\phi_{x,y} - \tilde{\phi}_{x,y} - \mu)^2 \qquad (20)$$

TABLE III
STANDARD DEVIATION BETWEEN ORIGINAL AND UNWRAPPED IMAGES

Image	Method	$\sigma_n = 0(0.00)$		$\sigma_n = 0.5(0.50)$		$\sigma_n = 1.0(1.00)$		$\sigma_n = 1.5(1.42)$	
		σ	σ'	σ	σ'	σ	σ'	σ	σ'
1	BLS	0.00	0.00	0.50	0.07	1.01	0.16	1.47	0.33
1	GR	0.00	0.00	0.50	0.08	1.57	1.27	3.20	3.00
1	MRM	-	0.03	-	0.08	-	1.26	-	2.97
2	BLS	0.00	0.12	0.50	0.14	1.01	0.20	1.47	0.36
2	GR	0.00	0.12	0.52	0.21	1.40	1.05	2.46	2.18
2	MRM	-	0.12	-	0.21	-	1.04	-	2.14

where σ is the standard deviation between the original image ϕ and the estimated, unwrapped, image $\tilde{\phi}$, and

$$\mu = \frac{1}{MN} \sum_{x=0}^{M-1} \sum_{y=0}^{N-1} \phi_{x,y} - \tilde{\phi}_{x,y}. \qquad (21)$$

M and N are the horizontal and vertical sizes of the images, respectively. For each slope/noise combination, 25 images were generated and unwrapped using the BLS method, with heuristic merging and block sizes four and eight. The mean of the standard deviations are reported for each slope/noise combination and block size.

B. Numerical Evaluation

Two synthetic images of size 256 × 256 pixels were generated. Image 1 had a parabolic intensity function with respect to the distance from the image center ($v = 18 - 0.000\,44d^2$, where d is the distance in pixels to the image center). Image 2 was the same image as Image 1, but the intensity in a circular area was increased with 2 to create a discontinuity in the image. Three levels of Gaussian noise were added to the images, and the images were wrapped into the principal interval $(-\pi, \pi]$. The mean of the noise was zero, and the standard deviations were 0.5, 1.0, and 1.5, respectively. Together with the noise-free images, this made a set of eight wrapped images. We compared the new BLS method with the GR and the MRM methods. These two methods use a pixel-by-pixel based least-squares approach, while the BLS method gives a block-by-block least-squares solution. The direct block merging scheme was used for the BLS method, and the block size was set to 8 × 8. For the MRM method, we used $\lambda = 5$. To compare the results, the standard deviations between the original noise free images and the unwrapped result images were calculated using (20).

The MRM method uses regularization and thus gives smoothed result images. A direct comparison of these images with the results of the BLS and GR methods is, therefore, not possible. To make a fair comparison, the resulting images of the BLS and GR methods were smoothed with a mean filter of size 7 × 7. The size of the filter was selected so that the extracted standard deviations from the three methods were approximately equal for the noise-free images.

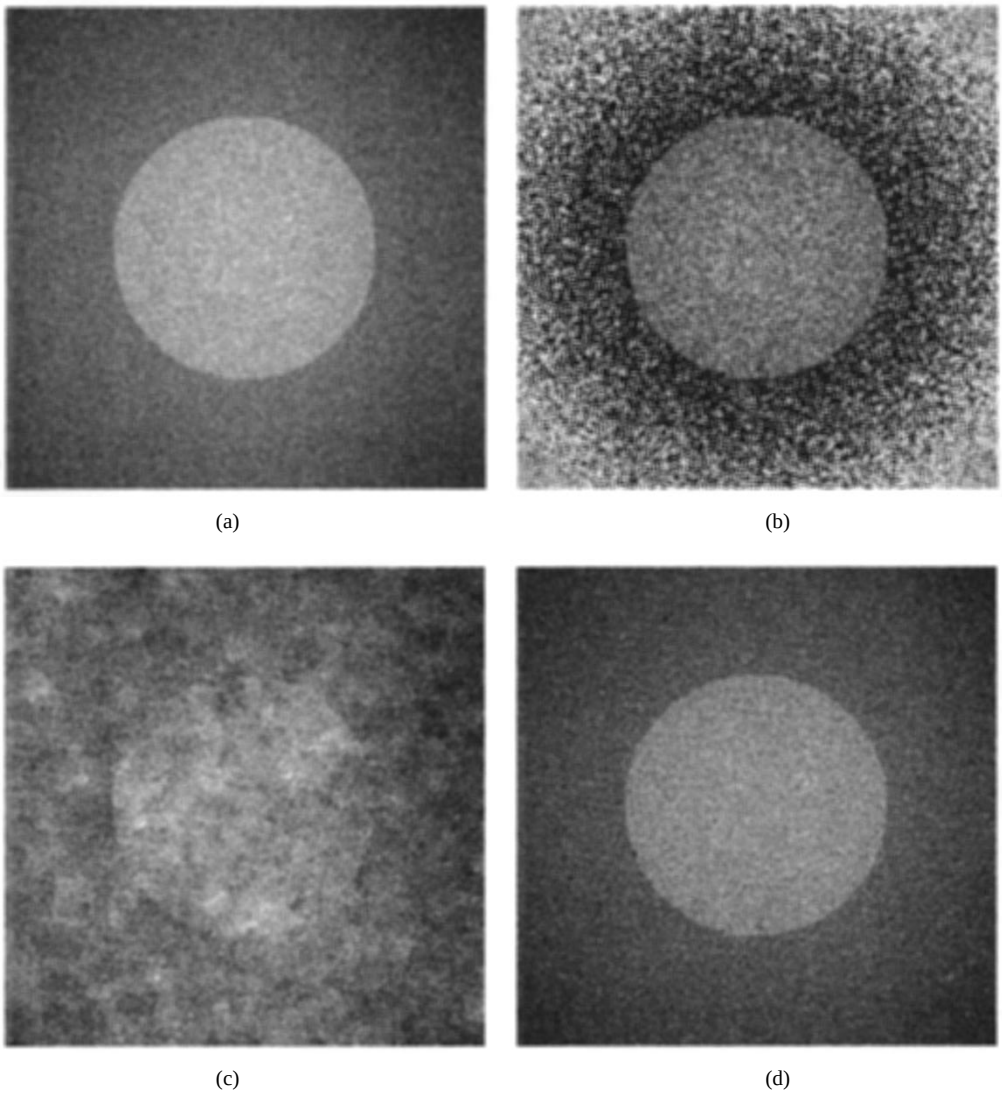

(a) (b) (c) (d)

Fig. 5. Phase unwrapping of Image 2. (a) Phase image with noise $\sigma = 1.0$ added. (b) Observed noisy wrapped image. (c) Unwrapped image using GR method. (d) Unwrapped image using BLS.

C. Versatility

In addition to the comparison with the other methods, we wanted to show the versatility of the new BLS method using the heuristic block merging scheme. We generated an image of a half scaled sphere and added Gaussian noise with zero mean and standard deviation 1.0. The shear in the image gradually increases from zero at the border of the sphere, to over 3π at the center of the sphere. A mask was, therefore, designed that excluded the pixels along the shear line. This image was unwrapped using a block size of 8×8. A fiber-optic interferometric image of a glass bunny was also tested. For this image, the mask was generated by taking the absolute value of the observed wrapped image, and then threshold the result. The block size was set to 8×8. Two MR images (field of view 300×300 mm, 256×256 samples) were recorded on a Siemens 0.95 Tesla MR scanner. The first image was a sagittal head image of a healthy volunteer, recorded with a Flash pulse sequence (TR = 25 ms, TE = 12 ms, flip angle 30°). The other image was a transversal head image of a healthy volunteer, recorded with a Turbo Spin Echo pulse sequence (TR = 2200 ms, TE = 25 ms, flip angle 90°). Masks were generated for these images by manually thresholding the corresponding amplitude images. The block size was set to 4×4 for the sagittal image, and 16×16 for the transversal image.

V. Results

A. Robustness

For noise levels with standard deviation 0.5 and smaller, the BLS method was very stable for all slope values (Tables I and II). With slope value one, and block size eight, high standard deviations were found for all noise levels. This was expected, since the sampling requirement of the block unwrapper was not valid for this case. The standard deviations increased with noise level and slope value.

B. Numerical Evaluation

The results of the three methods for Images 1 and 2 are summarized in Table III. In the table, the σ columns refer to the direct (not smoothed) results, while the σ' columns refer to

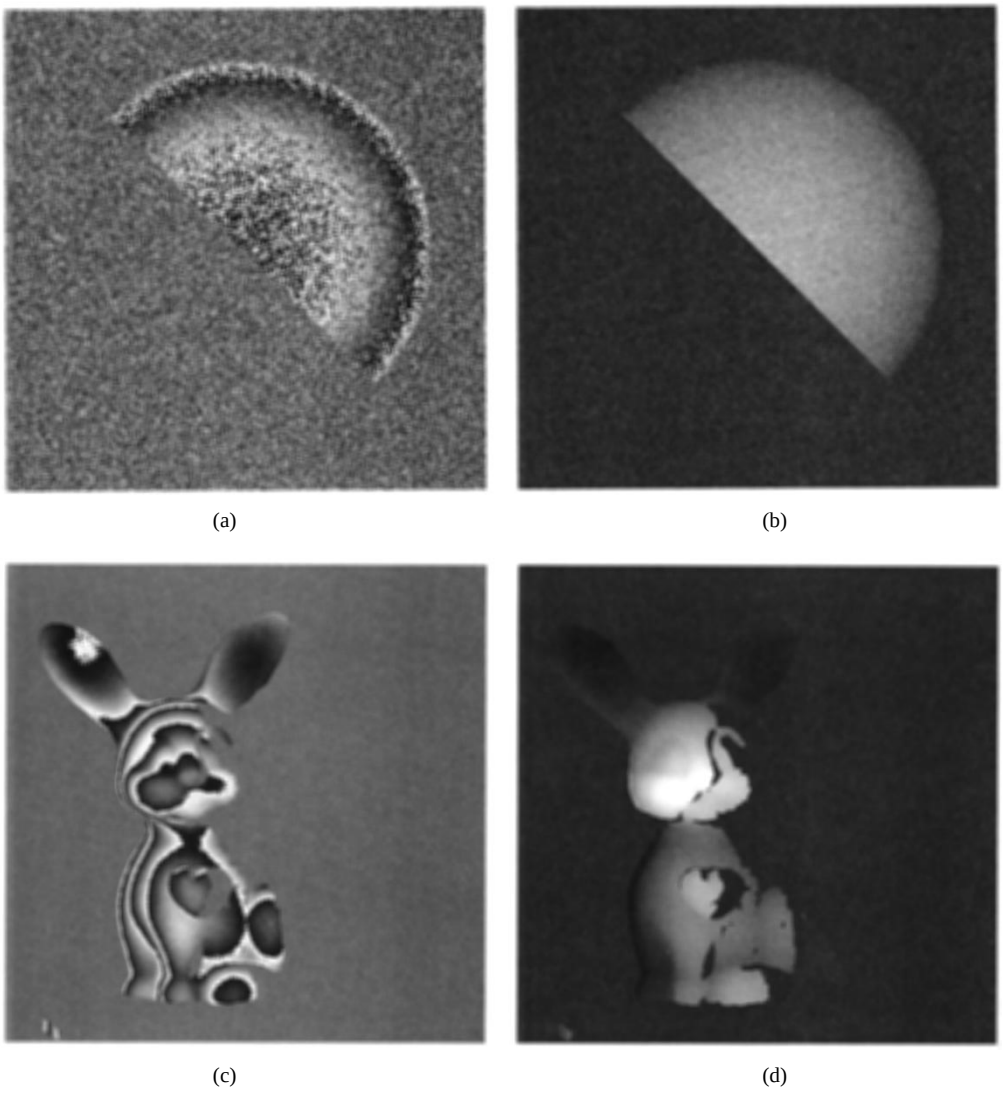

(a) (b)

(c) (d)

Fig. 6. Shear and bunny image. (a) Wrapped noisy image of a half scaled sphere. (b) Half sphere unwrapped. (c) Fiber-optic interferometry image of a bunny. (d) Bunny image unwrapped.

the results where the images from the BLS and GR methods were smoothed. For the direct results, we see that the BLS method gave images with standard deviations close to the added noise levels. The GR method had comparable results for low noise levels, but with higher noise levels the method resulted in very large standard deviations. For the smoothed results, the MRM method did not give as good results as the BLS and GR methods for low noise levels, while the BLS method was significantly better than the other methods for high noise levels. It is of interest to note that the differences between the smoothed GR results and the MRM results are very marginal. On a 143 MHz Sun UltraSPARC, the execution times were 1.5 s for the BLS method (not including possible reruns to find a suitable blocksize), and 7.1 s for the GR and the MRM methods.

Image 2 with noise level $\sigma = 1.0$ is shown in Fig. 5(a). The corresponding wrapped image is shown in Fig. 5(b). The visual differences between the results of the GR method [Fig. 5(c)] and of the BLS method [Fig. 5(d)] are striking. While the center disc is as clear as in the noisy original image for the BLS method, it is hardly visible for the GR method. The MRM output image looks like a smoothed version of the GR result. For the highest noise level, the disc was still clearly visible in the BLS result, while it was not visible at all for the GR and MRM methods.

We expect that the MRM method will produce better results if the λ value is tuned according to the noise level in the images. For instance, for no noise, $\lambda = 0$ will be a natural choice (which then makes the method equivalent to the GR method).

C. Versatility

The half scaled sphere [Fig. 6(a) and (b)], and the fiber-optic interferometry image of the glass bunny [Fig. 6(c) and (d)], were successfully unwrapped using BLS with the heuristic block merging scheme. Fig. 7(a) and (e) show the amplitude of the two MR images. The corresponding phase images are shown in Fig. 7(b) and (f). We see that the BLS method successfully unwrapped the images [Fig. 7(c) and (g)]. To show the details of the unwrapped phase images, the linear

phase component of the images was estimated using linear regression. The linear phase component was then subtracted from the unwrapped images. The results are shown in Fig. 7(d) and (h) (the background of the images were set to zero to better show the details inside the head). For MR images, we found that the BLS method was sensitive with respect to the mask definition. In general, it was better to include much of the noisy background pixels just outside the object when thresholding the amplitude images to generate the masks. Sagittal head images were especially sensitive, probably because of the magnetic susceptibilities and the complex geometry in the head at this slice direction. For transversal images, the BLS method was less sensitive with respect to the mask.

VI. Discussion and Conclusions

The block least-squares method for 2-D phase unwrapping has been presented and evaluated. The method works by first tessellating the images into small blocks with only one wrap in each block. A simple procedure is used to unwrap the blocks. The blocks are then merged together using one of the two suggested block merging algorithms. In a comparison with the methods of Ghiglia–Romero method and the Marroquin–Rivera method, the standard deviations between the original and the unwrapped images were calculated. The standard deviations for the BLS method were much lower than for the other two methods in images with high noise levels. With low noise levels, the differences between the methods were smaller. Also visually the results of the BLS method were shown to be superior to the other two methods. The BLS method is fast. For the synthetic images used in the evaluation, the BLS method was over four times as fast as the GR and MRM methods. In addition to the numerical evaluation, the BLS method has been tested on several image types. Synthetic images with shears, fiber-optic interferometry images, and MR images were all successfully unwrapped.

A distinct difference between the BLS method and many other phase unwrapping methods is that no phase derivatives need to be estimated. To correctly estimate the phase derivatives, the observed differences must be less than π. This condition is often not met in practice because of noise in the images. Since the BLS method unwraps each block without estimating the derivatives, it is more robust to noise than many other methods. For methods that estimate the derivatives directly in the observed wrapped images, a bias in the estimated derivatives will be present in areas with nonzero gradients because of noise [35]. Thus, the BLS method avoids the bias problem in the block unwrapping since no derivatives are estimated. Marroquin *et al.* [36] proposed a method that uses Markov random fields. Like the BLS method, this method is capable of handling phase differences larger than π between neighbor pixels. The computational load, however, is significantly larger than the BLS method.

The block merging can be considered as an integration process. In contrast to other integration based methods [3], [6], [12]–[14], the integration is on a block by block basis (instead of a pixel by pixel basis), which also makes the method robust to noise because the merging is a least squares fit based on many pixel pairs. However, while the derivative bias errors are avoided in the block unwrapping, they still represent a problem for the merging part of the BLS method since differences between neighbor pixels are used. Thus, the BLS method are

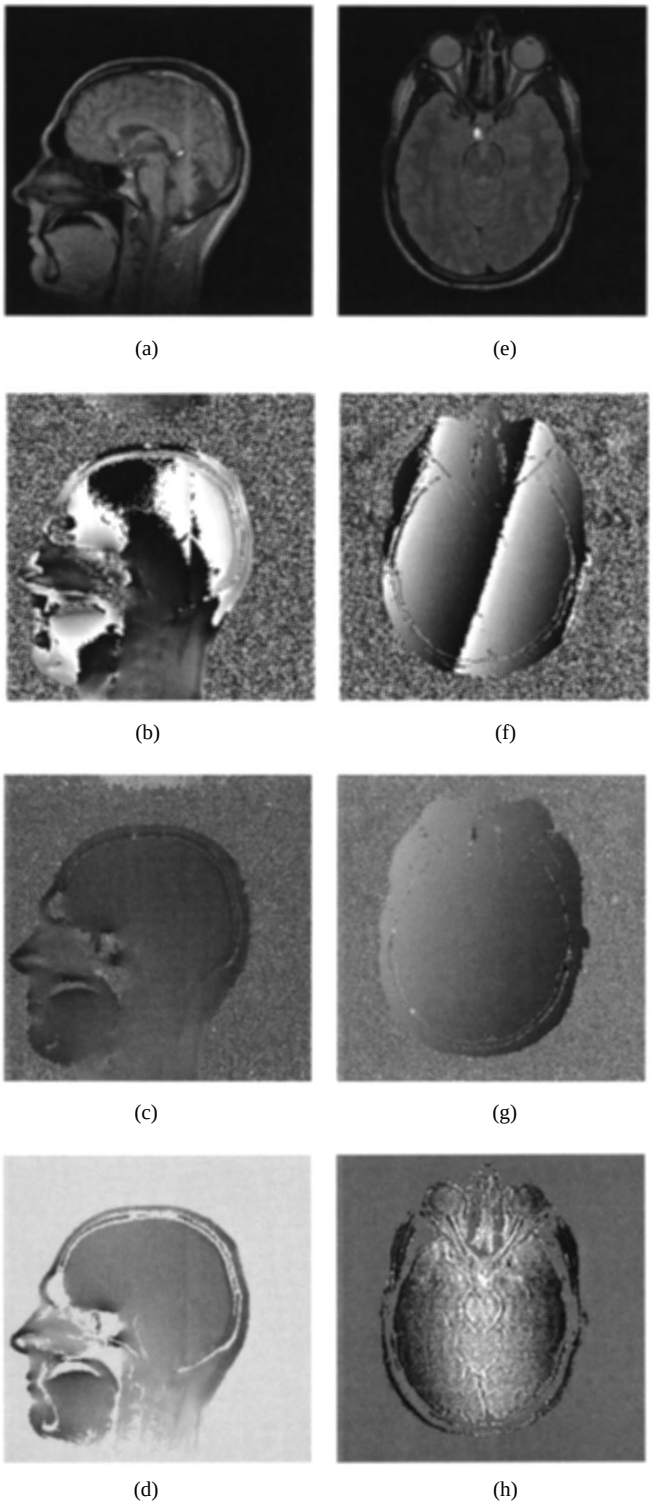

Fig. 7. Unwrapping of MR images. (a) Amplitude of sagittal head image. (b) Phase of sagittal head image. (c) Sagittal head image (b) unwrapped. (d) Unwrapped sagittal head image (c) with linear phase plane removed. (e) Amplitude of transversal head image. (f) Phase of transversal head image. (g) Transversal head image (f) unwrapped. (h) Unwrapped transversal head image (g) with linear phase plane removed.

not guaranteed to handle non masked undersampled areas, or areas with high gradients and much noise.

A clear advantage of the BLS method is that no boundary conditions are assumed on the unwrapped images. This is in contrast to many least-squares based methods (e.g., [19], [21]).

Least-squares method like the GR [19] and the MRM [21] methods are able to interpolate phase values in regions with no data in the images. An assumption about the derivatives in those areas must then be made. This will also influence the result in areas with data. These methods elegantly handles erroneous derivative estimates, since the least-squares expression is minimized for the whole image. The disadvantage is the loss of integrity (congruence modulo 2π). For many applications, like surface inspection using interferometry systems, the loss of integrity is not acceptable. In such cases, it may be better to mask out areas that cause problems, and get a reliable, congruent, unwrapped result for the remaining parts of the image using the BLS method.

The block size must be chosen based on the sampling density of the image, the complexity of the imaged object, and the noise level in the image. Small block sizes need much processing time, but may be required if the sampling density is low compared to the complexity of the imaged object. With much noise in the images, larger block sizes much be applied. Both the block unwrapping, and the block merging processes will then become more robust to noise.

For complex valued images, the mask required to unwrap nonrectangular objects can often easily be generated by thresholding the corresponding amplitude image. We found that the method was sensitive with respect to the mask definition, especially for objects of complex geometric form and with much noise. In such cases it is also hard to find a good threshold value to generate a mask. A too high threshold value will include points outside the imaged object in the mask. A too low threshold value will result in holes or gaps in the mask. In our experiments we selected a threshold value such that also some of the image points outside the imaged object became part of the mask. Another strategy may be to use a lower threshold value, and then use a morphological closing operation to improve the mask (e.g., [28], [37]).

In conclusion, the presented new block least-squares method for 2-D phase unwrapping has been shown to be better than other least-squares based methods on a limited set of images. We believe it has a large potential to improve the present quality of phase unwrapped images of several image modalities.

REFERENCES

[1] S. Dupont, D. Labrousse, and M. Berthod, "SAR interferometry: An application of simulated annealing to phase unwrapping," in *Proc. 9th Scandinavian Conf. Image Analysis*, 1995, pp. 697–705.

[2] G. Fornaro, G. Franceschetti, and R. Lanari, "Interferometric SAR phase unwrapping using Green's formulation," *IEEE Trans. Geosci. Remote Sensing*, vol. 34, pp. 720–727, 1996.

[3] R. M. Goldstein, H. A. Zebker, and C. L. Werner, "Satellite radar interferometry: Two-dimensional phase unwrapping," *Radio Sci.*, vol. 23, pp. 713–720, 1988.

[4] D. Massonet and T. Rabaute, "Radar interferometry: Limits and potential," *IEEE Trans. Geosci. Remote Sensing*, vol. 31, pp. 455–464, 1993.

[5] C. R. Mercer and G. Beheim, "Fiber-optic projected-fringe digital interferometry," in *Proc. Fall Conf. Hologram Interferometry and Speckle Metrology*, 1990.

[6] M. Hedley and D. Rosenfeld, "A new two-dimensional phase unwrapping algorithm for MRI images," *Magnet. Res. Med.*, vol. 24, pp. 177–181, 1992.

[7] S. Moon-Ho Song, S. Napel, N. J. Pelc, and G. H. Glover, "Phase unwrapping of MR phase images using Poisson equation," *IEEE Trans. Image Processing*, vol. 4, pp. 667–676, 1995.

[8] I. R. Young and G. M. Bydder, "Phase imaging," in *Magnetic Resonance Imaging*, D. D. Stark and W. G. Bradley, Eds. St. Louis, MO: Mosby Year Book, 1992, ch. 9.

[9] A. V. Oppenheim and R. W. Schafer, *Discrete-Time Signal Processing.* Englewood Cliffs, NJ: Prentice-Hall, 1989.

[10] J. Y. Wang, "Optical resolution through a turbulent medium with adaptive phase compensations," *J. Opt. Soc. Amer.*, vol. 67, pp. 383–390, 1977.

[11] M. H. Lee, J. F. Holmes, and J. R. Kerr, "Statistics of speckle propagation through the turbulent atmosphere," *J. Opt. Soc. Amer.*, vol. 66, pp. 1164–1172, 1976.

[12] J. M. Tribolet, "A new phase unwrapping algorithm," *IEEE Trans. Acoust., Speech, Signal Processing*, vol. ASSP-25, pp. 170–177, 1977.

[13] D. J. Bone, "Fourier fringe analysis: The two-dimensional phase unwrapping problem," *Appl. Opt.*, vol. 30, pp. 3627–3632, 1991.

[14] J. M. Huntley, "Noise-immune phase unwrapping algorithm," *Appl. Opt.*, vol. 28, pp. 3268–3270, 1989.

[15] G. Fornaro, G. Franceschetti, R. Lanari, and E. Sansosti, "A theoretical analysis on the robust phase unwrapping algorithms for SAR interferometry," in *Proc. Int. Symp. Geoscience and Remote Sensing*, 1996, pp. 2047–2049.

[16] D. L. Fried, "Least-square fitting a wave-front distortion estimate to an array of phase-difference measurements," *J. Opt. Soc. Amer.*, vol. 3, p. 67, 1977.

[17] R. H. Hudgin, "Wave-font reconstruction for compensated imaging," *J. Opt. Soc. Amer.*, vol. 67, pp. 375–378, 1977.

[18] B. R. Hunt, "Matrix formulation of the reconstruction of phase values from phase differences," *J. Opt. Soc. Amer. A*, vol. 69, pp. 393–399, 1979.

[19] D. C. Ghiglia and L. A. Romero, "Robust two-dimensional weighted and unweighted phase unwrapping that uses fast transforms and iterative methods," *J. Opt. Soc. Amer. A*, vol. 11, pp. 107–117, 1994.

[20] M. D. Pritt and J. S. Shipman, "Least-squares two-dimensional phase unwrapping using FFT's," *IEEE Trans. Geosci. Remote Sensing*, vol. 32, pp. 706–708, 1994.

[21] J. L. Marroquin and M. Rivera, "Quadratic regularization functionals for phase unwrapping," *J. Opt. Soc. Amer. A*, vol. 12, pp. 2393–2400, 1995.

[22] B. Friedlander and J. M. Francos, "Model based phase unwrapping of 2-D signals," *IEEE Trans. Signal Processing*, vol. 44, pp. 2999–3007, 1996.

[23] Z.-P. Liang, "A model-based method for phase unwrapping," *IEEE Trans. Med. Imag.*, vol. 15, no. 6, pp. 893–897, 1996.

[24] J. Leitão and M. A. Figueiredo, "Interferometric image reconstruction as a nonlinear Bayesian estimation problem," in *Proc. Int. Conf. Image Processing 95*, pp. 453–456.

[25] K. Itoh, "Analysis of the phase unwrapping algorithm," *Appl. Opt.*, vol. 21, p. 2470, 1982.

[26] W. F. Ames, *Numerical Methods for Partial Differential Equations.* New York: Academic, 1992.

[27] W. H. Press, S. A. Teukolsky, W. T. Vetterling, and B. P. Flannery, *Numerical Recipes in C.* Cambridge, U.K.: Cambridge Univ. Press, 1992.

[28] D. C. Ghiglia and M. D. Pritt, *Two-Dimensional Phase Unwrapping.* New York: Wiley, 1998.

[29] R. C. Gonzalez and P. Wintz, *Digital Image Processing.* Reading, MA: Addison Wesley, 1987.

[30] R. V. Churchill and J. W. Brown, *Complex Variables and Applications.* New York: McGraw-Hill, 1990.

[31] N. Metropolis *et al.*, "Equations of state calculations by fast computing machines," *J. Chem. Phys.*, vol. 21, pp. 1087–1091, 1953.

[32] J. S. Lim, *Two-Dimensional Signal and Image Processing.* Englewood Cliffs, NJ: Prentice-Hall, 1990.

[33] G. H. Golub and C. F. Van Loan, *Matrix Computations.* Baltimore, MA: The John Hopkins Univ. Press, 1989.

[34] H. Gudbjartsson and S. Patz, "The Rician distribution of noisy MRI data," *Magnet. Res. Med.*, vol. 34, pp. 910–914, 1995.

[35] G. W. Davidson and R. Bamler, "A multiresolution approach to improve phase unwrapping," in *Proc. IGARSS '96 Int. Geoscience and Remote Sensing Symp.*, 1996, pp. 2050–2053.

[36] J. L. Marroquin, M. Tapia, R. Rodriguez-Vera, and M. Servin, "Parallel algorithms for phase unwrapping based on Markov random field models," *J. Opt. Soc. Amer. A*, vol. 12, pp. 2578–2585, 1995.
[37] M. Rivera, R. Rodriguez-Vera, and J. L. Marroquin, "Robust procedure for fringe analysis," *J. Opt. Soc. Amer. A*, vol. 36, pp. 8391–8396, 1997.

Jarle Strand received the M.Sc. degree in computer science from the University of Bergen, Norway, in 1995. He is currently pursuing the Ph.D. degree in statistics at the University of Bergen.

His main research interests include phase unwrapping, statistical image restoration, and texture analysis.

Torfinn Taxt (M'88) was born in 1950. He received the M.Sc. degrees in computer science in 1978, the Ph.D. degree in developmental neuroscience in 1983, and the M.D. degree in 1976, all from the University of Oslo, Norway.

He is a Professor of image processing at the University of Oslo and a Professor of biomedical imaging at the University of Bergen, Norway. His primary research interests are restoration, segmentation, and multispectral analysis applied to medical ultrasound, and magnetic resonance images. He has also published papers on image models, satellite remote sensing, sonars, and document processing. He has more than 70 international publications in neuroscience, image processing, and pattern recognition.

Dr. Taxt is an Associate Editor of IEEE TRANSACTIONS ON MEDICAL IMAGING and *Pattern Analysis and Applications.*

Anil K. Jain (S'70–M'72–SM'86–F'91) received the B. Tech. degree in 1969 from the Indian Institute of Technology, Kanpur, India, and the M.S. and Ph.D. degrees in electrical engineering from The Ohio State University, Columbus, in 1970 and 1973, respectively.

He is a University Distinguished Professor and Chair of the Department of Computer Science and Engineering, Michigan State University, East Lansing. His research interests include statistical pattern recognition, Markov random fields, texture analysis, neural networks, document image analysis, fingerprint matching, and 3-D object recognition.

Dr. Jain was Editor-in-Chief of the IEEE TRANSACTIONS ON PATTERN ANALYSIS AND MACHINE INTELLINGENCE. He is co-author of *Algorithms for Clustering Data* (Englewood Cliffs, NJ: Prentice-Hall, 1988).He is editor of *Real-Time Object Measurement and Classification* (Berlin, Germany: Springer-Verlag, 1988). He is co-editor of *Analysis and Interpretation of Range Images* (Berlin, Germany: Springer-Verlag, 1988), *Markov Random Fields* (New York: Academic, 1992), *Artificial Neural Networks and Pattern Recognition* (Amsterdam, The Netherlands: Elsevier, 1993), *3-D Object Recognition* (Amsterdam, The Netherlands: Elsevier, 1993), and *Biometrics: Personal Identification in Networked Society* (Boston, MA: Kluwer, 1998). He received the Best Paper Awards in 1987 and 1991 and certificates for outstanding contributions in 1976, 1979, 1992, and 1997, from the Pattern Recognition Society. He also received the 1996 IEEE TRANSACTIONS ON NEURAL NETWORKS Outstanding Paper Award. He received a Fulbright Research Award in 1998. He is a Fellow of IAPR.